

Constraints on FRB emission in the aftermath of GRBs

B. Patricelli^{1,2,3}, M.G. Bernardini⁴ *, and M. Ferro^{4,5}

¹ Physics Department, University of Pisa, Largo B. Pontecorvo 3, I-56127 Pisa, Italy
e-mail: barbara.patricelli@pi.infn.it

² INFN - Pisa, Largo B. Pontecorvo 3, I-56127 Pisa, Italy

³ INAF - Osservatorio Astronomico di Roma, Via Frascati 33, I-00078 Monte Porzio Catone (Rome), Italy

⁴ INAF - Osservatorio Astronomico di Brera, via Bianchi 46, I-23807 Merate (LC), Italy
e-mail: maria.bernardini@inaf.it

⁵ Università degli Studi dell'Insubria, Dipartimento di Scienza e Alta Tecnologia, Via Valleggio 11, I-22100 Como, Italy

ABSTRACT

Context. Fast Radio Bursts (FRBs) are highly energetic radio transients with millisecond duration, whose physical origin is still unknown. Many models consider magnetars as possible FRB sources, supported by the observational association of FRBs with the galactic magnetar SGR 1935+2154. Magnetars are also thought to be the source of the power of a fraction of Gamma Ray Bursts (GRBs), opening the possibility that the two extreme phenomena have a common progenitor.

Aims. In this work we put constraints to this hypothesis searching for possible associations between GRBs and FRBs with currently available catalogs, and estimating if the lack of coincident detection can rule out their association.

Methods. We cross-matched all the Swift GRBs detected so far with all the well-localised FRBs reported in the FRBSTATS catalog, and we looked for FRB-GRB associations considering both spatial and temporal constraints. We also simulated a synthetic population of FRBs associated with Swift GRBs to estimate how likely it is to have a joint detection with current and future radio facilities.

Results. We recover two, low significant, possible associations already reported in literature from the catalogs' matches: GRB 110715A/FRB 20171209A and GRB 060502B/FRB 20190309A. However, our study shows that the absence of any unambiguous association so far between Swift GRBs and FRBs cannot exclude that the two populations are connected, given the characteristics of current GRB and FRB detectors.

Conclusions. Currently available observational data are not sufficient to clearly exclude/confirm whether GRBs and FRBs are physically associated. In the next decade, with new generations of GRB and FRB detectors there will be a higher probability to detect joint GRB-FRB events, if any; future observations will therefore be key to put more stringent constraints on the hypothesis that FRBs and GRBs have common progenitors.

Key words. Gamma-ray burst: general – Stars: magnetars

1. Introduction

Fast radio bursts (FRBs) are millisecond-duration radio bursts discovered more than a decade ago (Lorimer et al. 2007). To date, hundreds of FRBs have been detected at frequencies ranging between 400 MHz - 8 GHz by several ground-based radio telescopes (see, e.g., CHIME/FRB Collaboration et al. 2021). Some of them have been shown to repeat (Spitler et al. 2016; Kumar et al. 2019; CHIME/FRB Collaboration et al. 2019; Chime/Frb Collaboration et al. 2023). All the observed FRBs have large dispersion measures (DMs), suggesting an extragalactic origin (Lorimer et al. 2007; Thornton et al. 2013; Cordes & Chatterjee 2019). This has been proven by the identification of the host galaxy of FRB 121102, characterized by a redshift $z=0.1932$ (Chatterjee et al. 2017; Tendulkar et al. 2017).

The physical origin of FRBs is not established, especially because of the lack of an observed counterpart at other wavelengths. The only exception is the detection of a bright radio burst reported by the CHIME/FRB Collaboration et al. (2020) and by the STARE2 radio array (Bochenek et al. 2020) spatially and temporally coincident with an X-ray burst from the Galactic magnetar SGR 1935+2154 (Mereghetti et al. 2020), establishing the first direct link between magnetars and FRBs. Other evi-

dences supporting the magnetar origin for FRBs come from the properties of the host galaxy of the first repeating FRB 121102 (Tendulkar et al. 2017; Bassa et al. 2017) and the discovery of a persistent radio synchrotron source spatially coincident with it (Marcote et al. 2017) that point to a young magnetar born from a catastrophic event, such as superluminous supernovae (SLSNe) and long gamma-ray bursts (GRBs, Metzger et al. 2017; Nicholl et al. 2017). This has been confirmed by FRB 20180916B (Marcote et al. 2020; Tendulkar et al. 2021) and FRB 20201124A (Nimmo et al. 2022), although FRB 20200120E has been localised in a globular cluster (Kirsten et al. 2022; Nimmo et al. 2023).

Both long and short GRBs have been suggested to be powered by magnetars (Dai & Lu 1998; Zhang & Mészáros 2001; Corsi & Mészáros 2009; Metzger et al. 2011). This proposal has been revealed itself very successful in reproducing different observed properties of the X-ray emission of GRBs, at least from a phenomenological point of view (Metzger et al. 2008; Dall'Osso et al. 2011; Bucciantini et al. 2012; Rowlinson et al. 2013; Bernardini et al. 2013; Gompertz et al. 2014; Bernardini 2015; Stratta et al. 2018; Dall'Osso et al. 2023). The merger of binary systems of compact objects containing at least one neutron star have been proved to be the progenitors of short GRBs

* The first two authors equally contributed to this work

(Abbott et al. 2017) and at least of a fraction of long GRBs (Rastinejad et al. 2022).

Many FRB progenitor models¹ proposed in the last years advocate scenarios that hint to a possible association with GRBs. Such models can be grouped in two main categories: non-catastrophic models (mainly related to repeating FRBs) and catastrophic models (mainly related to non-repeating FRBs). Non-catastrophic models include magnetar flares (e.g., Kulkarni et al. 2014; Margalit & Metzger 2018) and giant pulses from neutron stars (Cordes & Wasserman 2016); catastrophic models include the collapse of supramassive neutron stars (Zhang 2014; Falcke & Rezzolla 2014; Punsly & Bini 2016) and the merger of compact stars (Liu et al. 2016). Depending on the scenario considered, the FRB could occur from milliseconds before to up to years after the GRBs.

Several searches for a systematic association of FRBs with GRBs have been performed in the last years (e.g., Curtin et al. 2023; Ashkar et al. 2023), and only two possible associations have been found so far: FRB 20171209 with the long GRB 110715A, whose afterglow is consistent with being powered by a magnetar (Wang et al. 2020); FRB 20190309A with the short GRB 060502B (Lu et al. 2024). However, the statistical significance of both these associations is quite low.

In this work we perform a new, systematic search for GRB-FRB association using the most updated catalog of FRBs observed with the Canadian Hydrogen Intensity Mapping Experiment (CHIME) instrument, and the sample of all GRBs detected by Swift so far. In our search we used the precise localization of GRB afterglows, and we allowed a few years of time delay between a GRB and an FRB. The paper is organized as follows: in Sect. 2 we describe our search method and the results we found; in Sect. 3 we present a study to assess the significance of the results of our search to confirm/exclude the association between GRBs and FRBs; finally, in Sect. 4 we discuss our results and summarize our conclusions.

2. Search for GRB/FRB association using archival data

We selected² all the GRBs (both short and long) detected by Swift until March 2023 for which there is an XRT detection and, thus, the position is available with an accuracy $\sigma_{\text{GRB}} \lesssim 5''$ (1276 GRBs). We also drew from this sample a subsample of GRBs for which a reliable redshift measurement is available (400 GRBs). In order to extend the time window of research, we also considered a sample of pre-Swift GRBs (from BeppoSAX, HETE-II and INTEGRAL) which have a localization with accuracy $\sigma_{\text{GRB}} < 10''$ and the redshift (32 GRBs; the first one is GRB 970228).

We considered all the FRBs from the FRBSTATS Catalogue³ (Spanakis-Misirlis 2021) available until March 2023 (828 FRBs; the last one is FRB 20221128A), both repeating and non-repeating. Among those, we selected the FRBs with an accuracy in the localization⁴ $\sigma_{\text{FRB}} \leq 30'$ (633 FRBs).

¹ For a recent review see Platts et al. (2019) and https://frbtheorycat.org/index.php/Main_Page.

² https://swift.gsfc.nasa.gov/archive/grb_table/

³ <https://www.herta-experiment.org/frbstats/catalogue>

⁴ Although the error regions of FRBs are elliptical, for the well-localised case the distribution of $\delta = (\sigma_{\text{RA}} - \sigma_{\text{Dec}})/\sigma_{\text{Dec}}$ has a mean value $\mu_{\delta} = 0.15$ and standard deviation $\sigma_{\delta} = 1.1$. Thus, in what follows we approximate the error regions as circular.

We then searched for any Swift GRB that is spatially coincident with an FRB from the two samples described above, without any further restriction. In order to have a coincidence, we required that the distance between the two is smaller than 3σ , with $\sigma^2 = \sigma_{\text{GRB}}^2 + \sigma_{\text{FRB}}^2$, and in any case not larger than $30'$. We find 28 matches. However, the most likely scenarios are that the FRB is either coincident or follows the GRB event.

If we restrict to those cases where the FRB follows the GRB event, the positive matches are 21; these are shown in Fig. 1 and listed in table A.1. All the positive matches involve non-repeating FRBs. In two cases, the same GRB matches two different, close by FRBs (GRB 110223A with FRB 20190519H and FRB 20190609A, and GRB 090813 with FRB 20190425B and FRB 20190609B).

For those GRBs with redshift (6 out of 21 spatially coincident with an FRB), we can also use the information on the distance and compare it to the inferred redshift of the corresponding FRB, available in the FRBSTATS Catalogue. Specifically, since the FRB redshift is estimated from the DM, we required that the redshift of the GRB is at least lower than the one inferred for the FRB. We find that only two matches satisfy this criterion:

- GRB 110715A**, a long GRB at $z_{\text{GRB}}=0.82$, and **FRB 20171209A**⁵, a non-repeating FRB discovered by Parkes with an inferred distance of $z_{\text{FRB}} = 1.17$;
- GRB 060502B**, a short GRB at an estimated redshift $z_{\text{GRB}}=0.287$, and **FRB 20190309A**⁶, a non-repeating FRB discovered by CHIME with an inferred distance of $z_{\text{FRB}} = 0.32$.

The "candidate a" is already reported by Wang et al. (2020) with a low significance (2.28-2.55 σ). Interestingly, for its characteristics GRB 110715A has been associated with a magnetar central engine (Wang et al. 2020).

The "candidate b" is also already reported by Lu et al. (2024) with a chance probability of 0.05. The distance between the two events is $13'$, which is less than 1σ ($\sigma = 21'$). In addition, the two events have a very similar redshift. However, the redshift of the GRB is actually the one of a massive red galaxy that, using associative and probabilistic arguments, was suggested to be its host galaxy (Bloom et al. 2007). This association is debated, especially due to the extremely large offset (Church et al. 2011).

Therefore we re-analysed the coincidence of the GRB 060502B with the putative host galaxy. We downloaded the candidate field from the Pan-STARRS1 public archive⁷ in the r band. We computed the probability of chance coincidence (P_{cc}) for the putative host galaxy with respect to the best afterglow position for GRB 06052B. Following the prescriptions from O'Connor et al. (2022), given the r band host magnitude of ~ 19.2 mag (AB, hereafter), and the angular separation from the XRT localization of $\sim 17.8''$, we found that $P_{\text{cc}} \approx 0.10$, which is higher than the previous estimate (Bloom et al. 2007). Since the limiting magnitude in the field is ~ 23 mag, we cannot exclude the presence of other potential fainter hosts, consistent with the best localization of the GRB. However, Bloom et al. (2007) found that even with a deeper image there are no better potential associations in the region, reporting several sources marginally consistent with the XRT position with magnitudes ranging from 24 to 26 mag, excluding another possible coincident hosts down to magnitude ~ 26.5 mag. The presence of an extremely faint host (> 26.5 mag) beneath the position of the

⁵ <https://www.wis-tns.org/object/20171209a>

⁶ <https://www.chime-frb.ca/catalog/>

⁷ <https://outerspace.stsci.edu/display/PANSTARRS/>

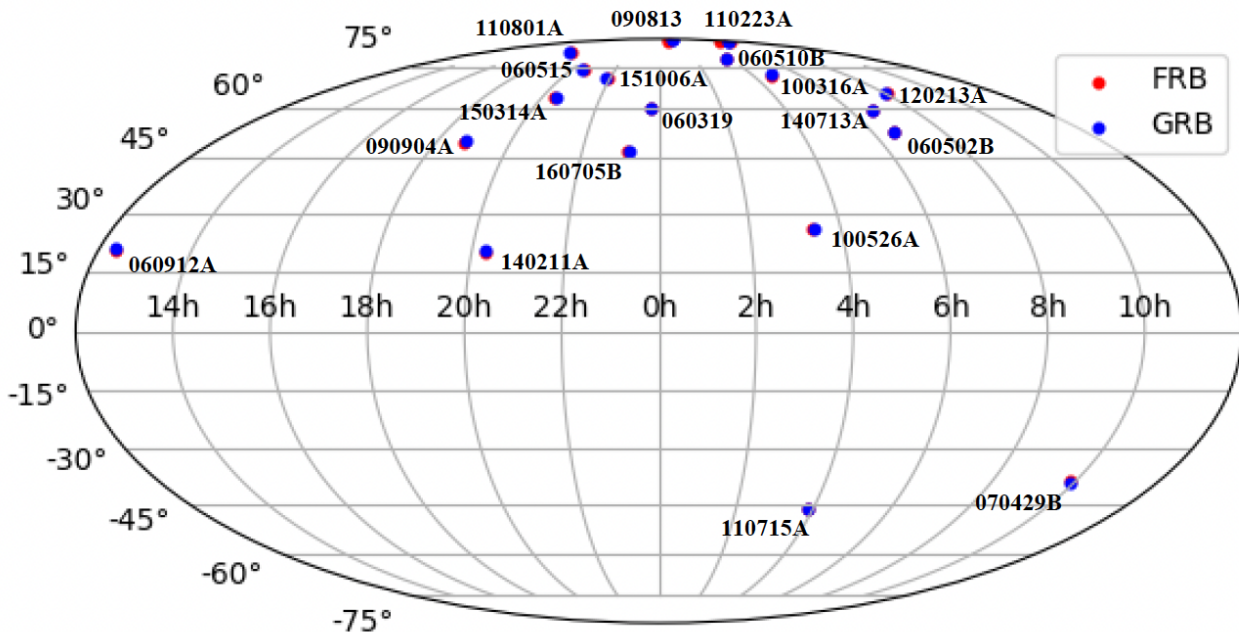


Fig. 1. FRBs and GRBs for which there is a positive match. The GRB names are also shown.

GRB, due to a higher redshift or because it is a red/dwarf galaxy as recently discussed for a sample of short GRBs by Nugent et al. (2024), cannot be ruled out.

Besides the low probability of association between GRB 060502B and the putative host galaxy at $z = 0.287$, Church et al. (2011) showed that a ≥ 70 kpc offset would be extremely difficult to attribute to the birth kick velocity, proposing a globular cluster nature for the birth site of the compact object binary system, which would guarantee the possibility of observing significantly larger offsets between the birth and merger sites. We also note that, according to the short GRB offset sample by Fong et al. (2022), GRB 060502B would be one of the outliers in the offset distribution, with $< 1\%$ of the events found at > 70 kpc.

We perform a further search for association between GRBs and FRBs with the pre-Swift GRBs with redshift, and we find 2 matches when considering only the spatial and temporal information:

- **GRB 030226**, a long GRB discovered by HETE-II at $z_{\text{GRB}}=1.98$, and **FRB 20190303C**, a non-repeating FRB discovered by CHIME with an inferred distance of $z_{\text{FRB}} = 1.09$;
- **GRB 051022**, a long GRB discovered by HETE-II at $z_{\text{GRB}}=0.81$, and **FRB 20190608A**, a non-repeating FRB discovered by CHIME with an inferred distance of $z_{\text{FRB}} = 0.68$;

However none of these matches is confirmed when accounting for the information on the distance, since in both cases the FRB is closer than the GRB.

2.1. Chance probability of the FRB/GRB association

Given the size of the samples of GRBs and FRBs considered in Sect. 2, we estimated the probability of having a specific number of GRB-FRB associations just by chance. To this aim, we proceeded as follows.

We restricted ourselves to the FRBs discovered by CHIME (516 out of 633 FRBs that we considered in Sect. 2) in order to better control the simulations with a homogeneous sample that

represents more than 80% of the FRBs of our original sample. We generated a synthetic population of 1276 GRBs and another one of 516 FRBs in the sky. We assumed GRBs and FRBs to have an isotropic and homogeneous distribution in space and, for FRBs, we restricted our simulations to the Northern hemisphere (Declination between -11 deg and 90 deg), to take into account the CHIME observable sky (see, e.g., CHIME/FRB Collaboration et al. 2021). We assumed that the uncertainty in the localization for the GRBs is negligible since the mean value of the accuracy in the localization for the GRBs detected and localised by Swift/XRT is $1.86''$. We extracted the uncertainty in the localization for the FRBs from a gaussian distribution with mean ($14.9'$) and standard deviation ($6.2'$) taken from the distribution for the CHIME FRBs with $\sigma_{\text{FRB}} \leq 30'$. We then assigned to each source a redshift, randomly extracted from the observed redshift distribution of Swift GRBs (https://swift.gsfc.nasa.gov/archive/grb_table/) and CHIME FRBs (CHIME/FRB Collaboration et al. 2021). We also assigned to each GRB a random occurrence time between November 20, 2004 (the starting time of Swift operations) and March 21, 2023; for FRBs, we considered a time interval between July 25, 2018, that is the starting date of the CHIME FRB catalog, and November 28, 2022, that corresponds to the most recent detected FRB reported in the catalog. To have enough statistics, we performed 10^5 realizations of the two above described populations.

For the entire population of GRBs, regardless of the information on the distance, we find that the distribution of the number of matches with FRBs has a mean value of 11.4 (median 11) and a standard deviation of 3.4. If we impose that the FRB follows the GRB, the mean value is 9.8 (median 10) with a standard deviation of 3.1. If we further require that the GRB is closer than the FRB, the mean value of the number of matches is 1.6 (median 1), with a standard deviation of 0.9.

In Sect. 2 we found only one match between CHIME FRBs and Swift GRBs, when applying the spatial, temporal and distance constraints. This is consistent with the expected number of chance coincidences. When considering only on spatial and

temporal constraints, the number of matches that we found (19 CHIME FRBs) is higher than the expected number of chance coincidences (see Fig. 2), although still consistent at a $3\text{-}\sigma$ level with expectations.

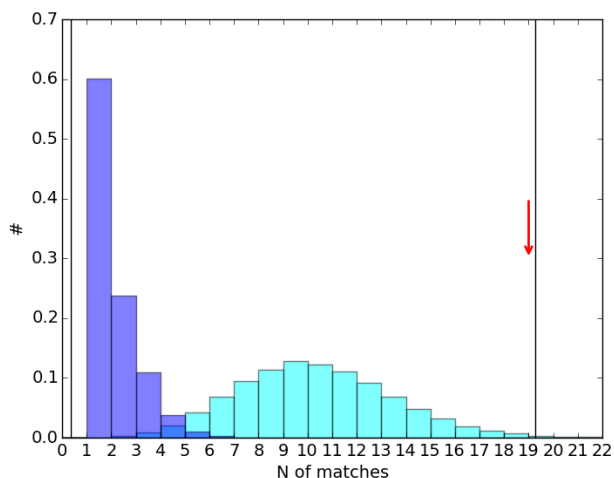


Fig. 2. Normalized distribution of the number of chance coincidences between GRBs and FRBs obtained by cross-matching the 10^5 realizations of GRB and FRB samples, when applying only spatial and temporal constraints (cyan) and when taking into account also the distance constraint (blue). The vertical solid lines mark the $3\text{-}\sigma$ confidence interval, and the vertical arrow marks the number of matches using real samples, when considering only spatial and temporal constraints.

3. Can we rule out the association between GRBs and FRBs?

Although there is no clear association between GRBs and FRBs, is this sufficient to exclude any connection between them? In other words, how likely is it to detect an FRB from a GRB under the hypothesis that all GRBs are associated with FRBs.

To answer this question, we started from the assumption that every GRB event is associated with an FRB without choosing an a-priori time delay since we are not relying on a specific model, and we estimated the detection rate of this population of FRBs. We only considered non-repeating FRBs, since they are more likely related to cataclysmic events of the same type as those originating GRBs. The inclusion of repeating FRBs requires a detailed modeling of the energy distribution and time-domain behaviour of bursts from a single source, and a dedicated analysis of the rates expected in this scenario will be investigated in a separate work.

To this end, we generated a synthetic population of 10^6 FRBs, assigning to each of them: i) a redshift; ii) a rest-frame isotropic energy.

i) The redshift was drawn from the redshift distribution of Swift GRBs, considering together both the short and long populations. This choice is motivated by the fact that here we are focusing only on the FRBs possibly associated with GRBs, that could represent only a subsample of the whole FRB population.

ii) The rest-frame isotropic energy was drawn from the FRB energy distribution $\Phi(E)$. The FRB luminosity and energy distributions have been investigated in the past by several authors, and they are typically assumed to follow a Schechter function (Schechter 1976). For instance, Luo et al. (2020) used a heterogeneous sample of 46 FRBs (both repeating and non-repeating)

observed with different instruments: Parkes, Arecibo, Green Bank Telescope, UTMOST and ASKAP and they measured the FRB luminosity function with a Bayesian approach, taking into account selection effects, such as the survey sensitivity; assuming a Schechter function and neglecting the cosmic evolution of FRBs, they found a slope of the luminosity function $\Phi(L)$ of $\alpha = -1.79^{+0.31}_{-0.35}$ and a lower cut-off luminosity $L_0 < 9.1 \times 10^{41}$ erg s^{-1} . Shin et al. (2023) used the full sample of 536 FRBs from the first CHIME catalog (CHIME/FRB Collaboration et al. 2021). They modeled the FRB energy distribution with a Schechter function and they assumed that $\Phi(E)$ does not evolve with redshift; they found a differential power-law index of $\alpha = -1.3^{+0.7}_{-0.4}$ and a characteristic exponential cut-off energy of $E_{char} = 2.38^{+5.35}_{-1.64} \times 10^{41}$ erg. Hashimoto et al. (2022, hereafter H22) used a homogeneous subsample of FRBs from the first CHIME catalog. They divided the selected FRBs in repeaters and non-repeaters, and then in several subsamples, filling different redshift bins covering the range between 0.05 and 3.6; since results may depend on how the redshift bins are selected, to take into account this uncertainty they performed their analysis considering two different sets of redshift bins (called “redshift A” and “redshift B”). They fitted Schechter functions to the derived energy functions and they took into account the redshift evolution. They found $\alpha = -1.4^{+0.7}_{-0.5}$ ($-1.1^{+0.6}_{-0.4}$) for redshift bin A (redshift bin B). Similar results are also presented in other papers (see, e.g., Lu & Piro 2019). Despite the different methodologies and different FRB samples used, the results found in the above described works are in broad agreement within errors. It is important to note that the observed energy and luminosity distributions could include the contribution from different FRB populations (e.g., having different progenitors), that could potentially have individual distributions different from each other.

In this work, we used the energy distribution derived by H22, and, as already mentioned, we considered non-repeating FRBs. Since the redshift range of GRBs is wider than the one considered in H22, we assumed that the energy distribution ($\phi(E)$) of FRBs with $z < 0.05$ (> 3.6) is the same obtained for the lowest (highest) redshift bin, and we considered both the redshift A and the redshift B cases, with the parameters reported in Table 1 of H22. We focused on the CHIME survey, since it is currently the one with the best combination in terms of sensitivity and field of view (fov). We then associated to each FRB a rest-frame isotropic energy integrated over the bandwidth $\Delta\nu = 400$ MHz (the CHIME frequency width), $E_{rest,400}$. We assumed a fiducial value for the minimum FRB rest-frame energy of 10^{37} ergs, that is the minimum energy of the FRBs in the CHIME catalog, and a maximum value of 10^{50} ergs.

From these values, we computed the observed fluence F_ν in the CHIME frequency band (400 MHz - 800 MHz) as

$$F_\nu = \frac{(1+z)^{2-\gamma} E_{rest,400}}{4\pi d_L^2(z) \Delta\nu}, \quad (1)$$

where $d_L(z)$ is the luminosity distance at redshift z , estimated with the cosmological parameters from Planck Collaboration et al. (2016), $\Delta\nu$ is the frequency bandwidth (taken as 400 MHz) and γ is the FRB spectral index ($F \propto \nu^{-\gamma}$), that we assumed to be equal to 1.4 (see, e.g., Shin et al. 2023).

Then, to evaluate how many FRBs originating from GRBs can be detected with CHIME, we compared the values of F_ν with the completeness threshold (95% c.l.) of $F_{lim} = 5$ Jy ms to account for the different sources of sensitivity variation (CHIME/FRB Collaboration et al. 2021). The percentage of sim-

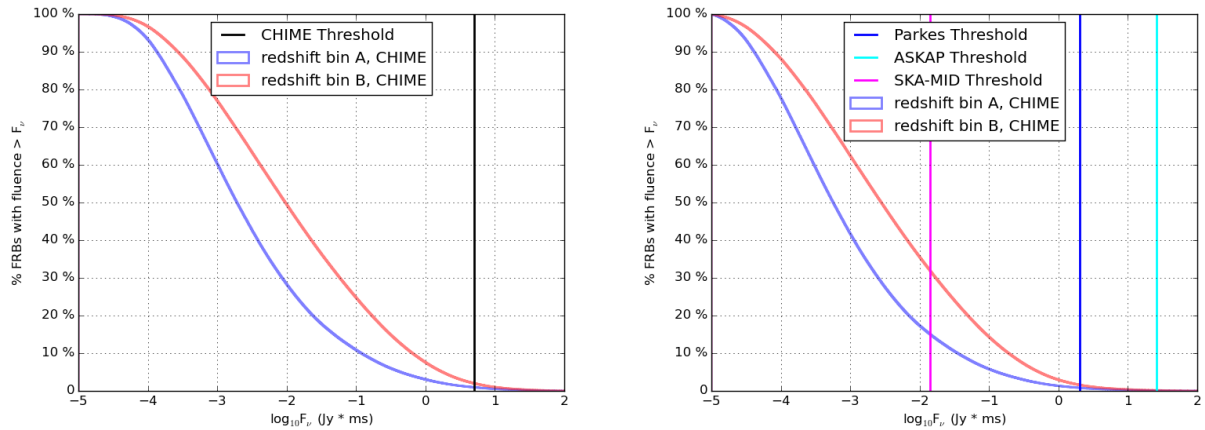


Fig. 3. Percentage of simulated FRBs with fluence greater equal than F_{γ} , vs F_{γ} , in the case of redshift bin A (in blue) and redshift bin B (in red). F_{γ} has been computed in the CHIME frequency band (left) and at 1.4 GHz (right). The vertical coloured lines mark the position of the assumed fluence threshold for CHIME, Parkes, ASKAP and SKA1-MID.

ulated FRBs with a fluence greater than $F_{\text{lim}} = 5 \text{ Jy ms}$ is 1% for redshift bin A, 2% for redshift bin B (see Fig. 3, left panel).

We then estimated the detection rate of FRBs associated with GRBs detected by Swift by multiplying these percentages to the Swift average detection rate (85 GRBs yr^{-1} discovered by BAT and 70 GRBs yr^{-1} detected also by XRT)⁸ and an instantaneous fov of $120^{\circ} \times 2^{\circ}$ (CHIME/FRB Collaboration et al. 2021), obtaining $R_{\text{FRB}} = [5 - 11] \times 10^{-3} \text{ yr}^{-1}$, where the lower and upper boundaries correspond to redshift bin A and B, respectively (see Table 1). These detection rates were obtained by assuming that each GRB is associated with one FRB, and this implicitly takes into account that there is a model-dependent time delay between the two events. Despite many uncertainties in the modelling of the FRB population and the simplified description of the detection process used, this result shows that the absence of a clear association between FRBs in the current (4 years) CHIME catalog and Swift GRBs cannot exclude that the two phenomena can have a common progenitor.

We then performed the same analysis considering Parkes and ASKAP; in this case, we evaluated the detection rates by calculating the observed fluence F_{γ} at 1.4 GHz and comparing it to the completeness threshold (95% c.l.) of $F_{\text{lim}} = 2$ and 26 Jy ms respectively (Bhandari et al. 2018; Shannon et al. 2018). The percentage of simulated FRBs with a fluence greater than F_{lim} is, respectively, 0.8% and 0.1% for redshift bin A, 1.7% and 0.3% for redshift bin B (see Fig. 3, right panel).

For Parkes: considering a duty cycle of 100% and a fov of 0.6 deg^2 (Luo et al. 2020) we obtain $R_{\text{FRB}} = [1-2] \times 10^{-5} \text{ yr}^{-1}$, where the lower and upper boundaries correspond to redshift bin A and B, respectively. For ASKAP: considering a duty cycle of 100% and a fov of 150 deg^2 (Luo et al. 2020) we obtain $R_{\text{FRB}} = [4 - 8] \times 10^{-4} \text{ yr}^{-1}$, where the lower and upper boundaries correspond to redshift bin A and B, respectively (see table 1).

It is important to highlight that the rates obtained in this work possibly underestimate the actual rates, since we do not consider in our analysis the population of repeating FRBs. The inclusion of repeating FRBs could increase the detection rates, since we would have multiple FRBs for each GRB.

Table 1. Detection threshold (F_{lim}), duty cycle (DC) and fov used to estimate the FRB detection rates with CHIME, Parkes, ASKAP and SKA1-Mid (Fender et al. 2015; Bhandari et al. 2018; Shannon et al. 2018; Luo et al. 2020; CHIME/FRB Collaboration et al. 2021).

	F_{lim} Jy ms	DC	fov deg^2	Det. rate yr^{-1}
CHIME	5	100	240	$[5-11] \times 10^{-3}$
Parkes	2	100	0.6	$[1-2] \times 10^{-5}$
ASKAP	26	100	150	$[4-8] \times 10^{-4}$
SKA1-MID	0.014	20	20	$[1-3] \times 10^{-3}$

4. Discussion and Conclusions

We performed a comprehensive search for possible association between GRBs and FRBs, cross-matching Swift/GRBs with all the FRBs reported in the FRBSTATS catalog. We initially applied only spatial and temporal constraints association, and then we also considered the distance information of the subsample of Swift/GRBs with known redshift. In this last case, we identify two matches: a) GRB 110715A/FRB 20171209A and b) GRB 060502B/FRB 20190309A. In previous searches (Wang et al. 2020) candidate ‘‘a’’ has already been reported as a low significance match. Candidate ‘‘b’’ is also already reported by Lu et al. (2024) with a statistical significance $< 3\sigma$; besides, the redshift estimate for the GRB is debated, further weakening the association. In any case, the number of matches found in our searches is consistent at a $3-\sigma$ level with the expectations from chance coincidences.

The absence of any unambiguous cross-match between the GRB and FRB catalogs cannot exclude that the two populations are connected. Indeed, even under the hypothesis that all GRBs are associated with a non-repeating FRBs, a survey with the same characteristics as CHIME would take hundreds of years to detect at least one FRB associated to a GRB discovered by Swift, as shown in Sect. 3. The expectations are even less promising when considering other current facilities such as Parkes and ASKAP.

Our results are valid for any delay time between GRBs and FRBs. However, our analysis can provide constraints only to models that predict a time delay between the two events from

⁸ https://swift.gsfc.nasa.gov/archive/grb_table/

zero to a few dozens of years, assuming a typical expected lifetime of instruments considered in this work. Much longer time delays cannot be probed with direct observations of the two phenomena.

The Square Kilometre Array (SKA) is a planned large radio interferometer designed to operate over a wide range of frequencies, and with an order of magnitude greater sensitivity and survey speed than any current radio telescope. The SKA will comprise two separate arrays, one in Western Australia and another in South Africa, and is designed to be built in phases. The first (SKA1) is expected to become fully operational by the late 2020's and should consist of three elements: one operating at low frequency (SKA1-LOW, [50-350] MHz), one at intermediate/high frequency (SKA1-MID, [1.2-1.7] GHz), and one optimized for surveys (SKA1-survey). For SKA1-MID, considering a completeness threshold of $F_{\text{lim}} = 0.014 \text{ Jy ms}$ (Fender et al. 2015) we obtain $R_{\text{FRB}} = [1 - 3] \times 10^{-3} \text{ yr}^{-1}$, where the lower and upper boundaries correspond to redshift bin A and B, respectively (see table 1). Therefore, despite its much higher sensitivity, the expectations for joint detection are comparable to CHIME performances, due to the smaller fov. However, in this work we considered the population of CHIME FRBs as representative of the whole population(s) of FRBs, which is not necessarily the case. With its higher sensitivity, SKA will probe the faint end of the FRBs' energy distribution, possibly discovering new features that are not accounted for in our model.

Besides, the derived rates are assuming that GRBs are associated with one-off FRBs. If instead they were connected with the population of repeaters, we would have multiple FRBs for one GRB, increasing the detection probability accordingly. As already mentioned in Sect. 3, a dedicated analysis of the rates expected in this scenario will be investigated in a separate work.

Another way to increase the probability of having a joint FRB-GRB detection is a more efficient GRB discovery machine, such as THESEUS (Amati et al. 2018). THESEUS is a space mission concept, selected by ESA as a candidate mission (launch in 2037), with the aim of exploiting GRBs for early Universe exploration and providing a fundamental contribution to time-domain and multi-messenger astrophysics. THESEUS will detect a factor ~ 10 more GRBs than Swift in the redshift range up to ~ 2.5 with accurate sky localization (Ghirlanda et al. 2021), which opens the possibility of observing a GRB associated to a detectable FRB by a facility with the same characteristics as CHIME within $\sim 10 \text{ yr}$ lifetime.

Acknowledgements. We acknowledge use of the CHIME/FRB Public Database, provided at <https://www.chime-frb.ca/> by the CHIME/FRB Collaboration. We thank Paolo D'Avanzo, Sara Elisa Motta and Sergio Campana for useful discussions.

References

- Abbott, B. P., Abbott, R., Abbott, T. D., et al. 2017, *ApJ*, 848, L13
- Amati, L., O'Brien, P., Götz, D., et al. 2018, *Advances in Space Research*, 62, 191
- Ashkar, H., El Bouhaddouti, M., Fegan, S., & Schüssler, F. 2023, *PoS, ICRC2023*, 555
- Bassa, C. G., Tendulkar, S. P., Adams, E. A. K., et al. 2017, *ApJ*, 843, L8
- Bernardini, M. G. 2015, *Journal of High Energy Astrophysics*, 7, 64
- Bernardini, M. G., Campana, S., Ghisellini, G., et al. 2013, *ApJ*, 775, 67
- Bhandari, S., Keane, E. F., Barr, E. D., et al. 2018, *MNRAS*, 475, 1427
- Bloom, J. S., Perley, D. A., Chen, H. W., et al. 2007, *ApJ*, 654, 878
- Bochenek, C. D., Ravi, V., Belov, K. V., et al. 2020, *Nature*, 587, 59
- Bucciantini, N., Metzger, B. D., Thompson, T. A., & Quataert, E. 2012, *MNRAS*, 419, 1537
- Chatterjee, S., Law, C. J., Wharton, R. S., et al. 2017, *Nature*, 541, 58
- CHIME/FRB Collaboration, Amiri, M., Andersen, B. C., et al. 2021, *ApJS*, 257, 59
- CHIME/FRB Collaboration, Amiri, M., Bandura, K., et al. 2019, *Nature*, 566, 235
- Chime/Frb Collaboration, Andersen, B. C., Bandura, K., et al. 2023, *ApJ*, 947, 83
- CHIME/FRB Collaboration, Andersen, B. C., Bandura, K. M., et al. 2020, *Nature*, 587, 54
- Church, R. P., Levan, A. J., Davies, M. B., & Tanvir, N. 2011, *MNRAS*, 413, 2004
- Cordes, J. M. & Chatterjee, S. 2019, *ARA&A*, 57, 417
- Cordes, J. M. & Wasserman, I. 2016, *MNRAS*, 457, 232
- Corsi, A. & Mészáros, P. 2009, 702, 1171
- Curtin, A. P., Tendulkar, S. P., Josephy, A., et al. 2023, *ApJ*, 954, 154
- Dai, Z. G. & Lu, T. 1998, 333, L87
- Dall'Osso, S., Stratta, G., Guetta, D., et al. 2011, *A&A*, 526, A121
- Dall'Osso, S., Stratta, G., Perna, R., De Cesare, G., & Stella, L. 2023, *ApJ*, 949, L32
- Falcke, H. & Rezzolla, L. 2014, *A&A*, 562, A137
- Fender, R., Stewart, A., Macquart, J. P., et al. 2015, in *Advancing Astrophysics with the Square Kilometre Array (AASKA14)*, 51
- Fong, W.-f., Nugent, A. E., Dong, Y., et al. 2022, *ApJ*, 940, 56
- Ghirlanda, G., Salvaterra, R., Toffano, M., et al. 2021, *Experimental Astronomy*, 52, 277
- Gompertz, B. P., O'Brien, P. T., & Wynn, G. A. 2014, *MNRAS*, 438, 240
- Hashimoto, T., Goto, T., Chen, B. H., et al. 2022, *MNRAS*, 511, 1961
- Kirsten, F., Marcote, B., Nimmo, K., et al. 2022, *Nature*, 602, 585
- Kulkarni, S. R., Ofek, E. O., Neill, J. D., Zheng, Z., & Juric, M. 2014, *ApJ*, 797, 70
- Kumar, P., Shannon, R. M., Osłowski, S., et al. 2019, *ApJ*, 887, L30
- Liu, T., Romero, G. E., Liu, M.-L., & Li, A. 2016, *ApJ*, 826, 82
- Lorimer, D. R., Bailes, M., McLaughlin, M. A., Narkevic, D. J., & Crawford, F. 2007, *Science*, 318, 777
- Lu, M.-X., Li, L., Wang, X.-G., et al. 2024, *ApJ*, 961, 45
- Lu, W. & Piro, A. L. 2019, *ApJ*, 883, 40
- Luo, R., Men, Y., Lee, K., et al. 2020, *MNRAS*, 494, 665
- Marcote, B., Nimmo, K., Hessels, J. W. T., et al. 2020, *Nature*, 577, 190
- Marcote, B., Paragi, Z., Hessels, J. W. T., et al. 2017, *ApJ*, 834, L8
- Margalit, B. & Metzger, B. D. 2018, *ApJ*, 868, L4
- Mereghetti, S., Savchenko, V., Ferrigno, C., et al. 2020, *ApJ*, 898, L29
- Metzger, B. D., Berger, E., & Margalit, B. 2017, *ApJ*, 841, 14
- Metzger, B. D., Giannios, D., Thompson, T. A., Bucciantini, N., & Quataert, E. 2011, 413, 2031
- Metzger, B. D., Quataert, E., & Thompson, T. A. 2008, 385, 1455
- Nicholl, M., Williams, P. K. G., Berger, E., et al. 2017, *ApJ*, 843, 84
- Nimmo, K., Hessels, J. W. T., Snelders, M. P., et al. 2023, *MNRAS*, 520, 2281
- Nimmo, K., Hewitt, D. M., Hessels, J. W. T., et al. 2022, *ApJ*, 927, L3
- Nugent, A. E., Fong, W.-f., Castrejon, C., et al. 2024, *ApJ*, 962, 5
- O'Connor, B., Troja, E., Dichiara, S., et al. 2022, *MNRAS*, 515, 4890
- Planck Collaboration, Ade, P. A. R., Aghanim, N., et al. 2016, *A&A*, 594, A13
- Platts, E., Weltman, A., Walters, A., et al. 2019, *Phys. Rep.*, 821, 1
- Punsly, B. & Bini, D. 2016, *MNRAS*, 459, L41
- Rastinejad, J. C., Gompertz, B. P., Levan, A. J., et al. 2022, *Nature*, 612, 223
- Rowlinson, A., O'Brien, P. T., Metzger, B. D., Tanvir, N. R., & Levan, A. J. 2013, *MNRAS*, 430, 1061
- Schechter, P. 1976, *ApJ*, 203, 297
- Shannon, R. M., Macquart, J. P., Bannister, K. W., et al. 2018, *Nature*, 562, 386
- Shin, K., Masui, K. W., Bhardwaj, M., et al. 2023, *ApJ*, 944, 105
- Spanakis-Misirlis, A. 2021, FRBSTATS: A web-based platform for visualization of fast radio burst properties, *Astrophysics Source Code Library*, record ascl:2106.028
- Spitler, L. G., Scholz, P., Hessels, J. W. T., et al. 2016, *Nature*, 531, 202
- Stratta, G., Dainotti, M. G., Dall'Osso, S., Hernandez, X., & De Cesare, G. 2018, *ApJ*, 869, 155
- Tendulkar, S. P., Bassa, C. G., Cordes, J. M., et al. 2017, *ApJ*, 834, L7
- Tendulkar, S. P., Gil de Paz, A., Kirichenko, A. Y., et al. 2021, *ApJ*, 908, L12
- Thornton, D., Stappers, B., Bailes, M., et al. 2013, *Science*, 341, 53
- Wang, X.-G., Li, L., Yang, Y.-P., et al. 2020, *ApJ*, 894, L22
- Zhang, B. 2014, *ApJ*, 780, L21
- Zhang, B. & Mészáros, P. 2001, 552, L35

Appendix A: GRBs and FRBs matches

Table A.1. List of GRBs and FRBs for which a match has been found (21 events) considering spatial and temporal constraints. The ones listed in the lower panel are those that also satisfy the distance constrain. All FRBs have been detected by CHIME with the exception of ^a from ASKAP and ^b from Parkes. The last column report the distance over σ between FRBs and GRBs.

GRB	z_{GRB}	RA deg	Dec deg	err "	FRB	z_{FRB}	DM	RA deg	Dec deg	err '	# σ
160705B	-	168.10942	46.69989	1.5	20180907E	0.4	381.7	167.88	47.09	19.94	1.3
151006A	-	147.42558	70.50303	1.5	20190612A	0.4	427.0	148.16	70.42	17.40	0.9
150314A	-	126.67042	63.83431	1.7	20190409B	0.3	297.6	126.65	63.47	18.25	1.2
140713A	-	281.10592	59.63347	1.4	20190429A	0.4	470.7	281.09	59.42	20.36	0.6
140211A	-	124.22329	20.24319	4.4	20190224C	0.4	495.0	124.05	19.78	17.84	1.7
120213A	-	301.01212	65.41131	1.4	20180918A	1.3	1454.1	301.27	64.96	17.84	1.6
110801A	1.9	89.43596	80.95631	1.5	20190208B	0.7	713.3	91.00	80.88	8.08	1.9
110223A	-	345.85217	87.55786	2.0	20190519H	1.1	1169.5	342.99	87.37	11.29	1.2
110223A	-	345.85217	87.55786	2.0	20190609A	0.3	315.4	345.30	87.94	25.97	0.9
100526A	-	230.76904	25.63219	1.7	20181221A	0.3	313.8	230.58	25.86	17.40	1.0
100316A	-	251.97875	71.82708	2.2	20190409C	0.6	674.5	252.60	71.62	19.53	0.9
090904A	-	100.88458	50.20289	1.6	20190317B	0.4	425.4	101.01	49.73	12.71	2.3
090813	-	225.78783	88.56822	1.4	20190425B	1.0	1030.3	210.12	88.60	13.96	1.7
090813	-	225.78783	88.56822	1.4	20190609B	0.3	292.8	210.49	88.35	9.86	2.8
070429B	0.9	328.01587	-38.82833	2.4	20180130A ^a	0.3	343.5	328.05	-38.57	17.20	0.9
060912A	-	5.28387	20.97181	1.4	20190316A	0.5	516.0	5.23	20.51	19.53	1.4
060515	-	127.28892	73.56778	3.5	20181213A	0.6	677.7	127.66	73.87	13.42	1.4
060510B	4.9	239.12192	78.56989	1.5	20181017B	0.3	304.1	237.76	78.50	20.38	0.8
060319	-	176.38767	60.01081	1.4	20181214C	0.6	632.4	175.93	60.02	7.75	1.8
110715A	0.8	237.68358	-46.23531	1.4	20171209A ^b	1.2	1457.4	237.60	-46.17	10.61	0.5
060502B	0.3	278.93846	52.63153	5.2	20190309A	0.3	357.5	278.96	52.41	19.94	0.7